

Sequential MAP Parametric OFDM Channel Estimation for Joint Sensing and Communication

Enrique T. R. Pinto and Markku Juntti

Centre for Wireless Communications (CWC), University of Oulu, Finland

{enrique.pinto, markku.juntti}@oulu.fi

Abstract—Uplink sensing is still a relatively unexplored scenario in integrated sensing and communication which can be used to improve positioning and sensing estimates. We introduce a pilot-based maximum likelihood, and a maximum a posteriori parametric channel estimation procedure using an orthogonal frequency division multiplexing (OFDM) waveform in uplink sensing. The algorithm is capable of estimating the multipath components of the channel, such as the angles of arrival, departure, path coefficient, and the delay and Doppler terms. As an advantage, when compared to other existing methods, the proposed procedure presents expressions for exact alternating coordinate updates, which can be further improved to achieve a competitive multipath channel estimation tool.

Index Terms—channel estimation, OFDM, uplink, sensing

I. INTRODUCTION

Radio-based sensing is being intensively studied for the purposes of joint sensing and communication (JSC). Exploiting the existing cellular infrastructure to perform sensing of passive devices, localization of active users, and mapping of the environment is not only economically attractive, it is also technically useful. Sensing, positioning, and environment data can not only be used to enhance mobile communications by improving power allocation, beamforming, and user scheduling, but it can also serve other systems such as autonomous vehicles and urban infrastructure by providing information for accident prevention, traffic flow optimization, etc.

As wireless communications standards progressively incorporate higher frequency ranges to their spectrum, such as frequency range 2 (FR2) in the fifth generation (5G) standard and also the very likely inclusion of sub-terahertz (subTHz) bands in beyond 5G (B5G) and sixth generation standard (6G), high mobility scenarios provide shorter and shorter channel coherence times. In these cases, channel state information (CSI) acquisition becomes a non-trivial problem, as channel estimates quickly become outdated due to Doppler shifts, thus, only estimating the channel matrix stops being an effective option. Extracting geometrical propagation information and using it as a deterministic (or hybrid) channel model can be a useful method [1], especially because it paves the way for channel prediction and environment sensing/mapping. If the propagation parameters of each multipath are well estimated, the line between sensing with mapping and channel estimation becomes blurred; these values allow us to approximately reconstruct the channel with a deterministic model instead of consigning propagation phenomena to stochastic terms. Furthermore, they provide essential information for JSC, which can be used

to detect passive sensing targets, map the environment, and enhance the position estimates of users.

In this paper, we propose a sequential maximum *a posteriori* (MAP) parametric channel estimation method for extracting the parameters of each multipath component of the channel in the context of *bistatic uplink sensing*. The most popular solution in non-real-time channel modelling applications is the space-alternating generalized expectation-maximization (SAGE) algorithm [2]. While generally successful, its alternating coordinate descent often rely on line-search procedures. This can limit its applicability in real-time scenarios. Other existing algorithms use the CANDECOMP/PARAFAC-decomposition (CP-decomposition) for a similar channel estimation procedure [3], [4]. However, they do not immediately exploit the structure of the channel tensor. Furthermore, the CP-decomposition is computationally expensive and outputs the best fitting rank K decomposition of the input tensor, requiring further processing for extracting channel parameters. In contrast, our proposed algorithm immediately outputs the channel parameters and exploits the channel model structure when computing their estimates, while also providing expressions for exact coordinate updates. This makes way for future work on improved channel estimation techniques that can further optimize the speed and accuracy of the channel parameter estimation process.

The rest of the paper is structured as follows. In Section II, we introduce the model considered in this paper. Then, in Section III, we present the chosen estimation approach. In Section IV, we introduce the necessary background for the optimization algorithm that is proposed in Section V. Finally, we analyse some numerical results in Section VI and make our concluding remarks in Section VII.

II. SYSTEM MODEL

Consider the following orthogonal frequency division multiplexing (OFDM) uplink received signal model [5]

$$\mathbf{y}_{n,t} = \sum_{\ell=1}^L b_{\ell} e^{-j2\pi n(\tau_{\ell} + \tau_o) f_c} e^{j2\pi t(f_{D,\ell} + f_o) T_s} \cdot \mathbf{a}(\phi_{\ell}) \mathbf{a}^T(\theta_{\ell}) \mathbf{x}_{n,t} + \mathbf{w}_{n,t}, \quad (1)$$

where n and t denote the OFDM subcarrier and symbol index, respectively; $\mathbf{y}_{n,t}$ is the signal received by the base station (BS) at the n th subcarrier and t th symbol; L is the number of multipath components; b_{ℓ} is the ℓ th path gain; τ_{ℓ} is the propagation delay of the ℓ th multipath; τ_o is the

clock timing offset between the user equipment (UE) and the BS; f_c is the subcarrier spacing B/N_c , where B is the bandwidth; $f_{D,\ell}$ is the Doppler frequency of the ℓ th multipath; f_o is the carrier frequency offset (CFO) of between UE and the BS; T_s is the OFDM symbol length; $\mathbf{a}(\phi/\theta)$ is the uniform linear array (ULA) response vector with N_r/N_t antennas and angle of arrival/departure ϕ/θ , given by $\mathbf{a}(\phi/\theta) = [1 \ e^{-j\pi \sin(\phi/\theta)} \ \dots \ e^{-j\pi(N_r/T-1)\sin(\phi/\theta)}]^T$, where “ ϕ/θ ” here denotes “either ϕ or θ ”; $\mathbf{x}_{n,t}$ is the transmitted pilot at the n th subcarrier and t th symbol; and finally \mathbf{w}_n is additive white Gaussian noise (AWGN) at the n th subcarrier and t th symbol with covariance $N_0\mathbf{I}_{N_r}$. Because the signal is transmitted by the UE, this scenario is called uplink sensing. Other variations of the uplink sensing also exist, those are based on setting up UEs, synchronized and with shared oscillator signals, deployed specifically for sensing. The model in (1) is general nonetheless, the dedicated UE scenario is readily obtained by setting the offsets to zero.

In a communications context, we are usually exclusively interested in the composited values of the channel matrices

$$\mathbf{H}_{n,t} = \sum_{\ell=1}^L b_\ell e^{j\omega_{1,\ell}n} e^{j\omega_{2,\ell}t} \mathbf{a}(\phi_\ell) \mathbf{a}^T(\theta_\ell), \quad (2)$$

where $\omega_{1,\ell} = -2\pi(\tau_\ell + \tau_o)f_c$ and $\omega_{2,\ell} = 2\pi(f_{D,\ell} + f_o)T_s$. However, in radio-based sensing and localization we are interested in estimating the sensing parameters $(b, \tau, f_D, \phi, \theta)$. Furthermore, the timing and frequency offset parameters $\xi_o = (\tau_o, f_o)$ are important to be estimated, because they lead to ranging and speed estimation ambiguity. It may be assumed that the offsets are the same for all the antennas, because the signal from the local oscillator (LO) is shared within the radio chains of an UE. In this work, we do not tackle the estimation of the offsets, instead we focus exclusively on estimating $\xi_\ell = (b_\ell, \omega_{1,\ell}, \omega_{2,\ell}, \phi_\ell, \theta_\ell) \forall \ell$. The offsets remain a nuisance and additional estimation methods would be required to identify them if the times-of-flight or Doppler frequencies are of interest.

III. MAXIMUM A POSTERIORI ESTIMATION

Define $\mathbf{y} = \text{vect}(y_{n,t,u})$, where $\text{vect}(\cdot)$ denotes the tensor vectorization operation, also denote by ξ the vector of sensing parameters ξ_ℓ for all detected paths, then the posterior of ξ given the data \mathbf{y} is

$$p(\xi|\mathbf{y}) = \frac{p(\mathbf{y}|\xi)p(\xi)}{p(\mathbf{y})} = \frac{\prod_{n,t,u} p(y_{n,t,u}|\xi)p(\xi)}{\int_{\Xi} \prod_{n,t,u} p(y_{n,t,u}|\xi')p(\xi')d\xi'}, \quad (3)$$

where Ξ denotes the parameter space and $p(\xi)$ denotes the prior for ξ . Throughout the remainder of this paper, summation and products over $n/t/u/v$ go from 0 to $N_{c/s/r/t} - 1$, unless otherwise indicated. The MAP estimate is then given by

$$\hat{\xi} = \underset{\xi}{\text{argmax}} p(\xi|\mathbf{y}) = \underset{\xi}{\text{argmax}} \prod_{n,t,u} p(y_{n,t,u}|\xi)p(\xi), \quad (4)$$

since the denominator of (3) is a constant. The conditional probability density function (PDF) of the data is complex

normal $y_{n,t,u}|\xi \sim \mathcal{CN}(\mu_{n,t,u}(\xi), N_0)$, where the mean is given by

$$\mu_{n,t,u}(\xi) = \sum_{\ell=1}^L b_\ell e^{j\omega_{1,\ell}n} e^{j\omega_{2,\ell}t} e^{-j\pi u \sin(\phi_\ell)} \mathbf{a}^T(\theta_\ell) \mathbf{x}_{n,t}. \quad (5)$$

The priors are assumed to be independent. Given the likelihood and prior, the log-posterior is

$$\begin{aligned} \log p(\xi|\mathbf{Y}) &= -\frac{1}{N_0} \sum_{n,t,u} |y_{n,t,u} - \mu_{n,t,u}(\xi)|^2 \\ &+ \sum_{\ell=1}^L \log(p(b_\ell)p(\omega_{1,\ell})p(\omega_{2,\ell})p(\phi_\ell)p(\theta_\ell)) + \dots, \end{aligned} \quad (6)$$

where we have omitted the constant terms.

IV. OPTIMIZATION PRELIMINARIES

We write the MAP estimation as a constrained minimization problem

$$\min_{\xi} \left[\frac{1}{N_0} \sum_{n,t,u} |y_{n,t,u} - \mu_{n,t,u}(\xi)|^2 - \log p(\xi) \right] \quad (7)$$

$$\text{s.t. } \angle b_\ell, \omega_{1,\ell}, \omega_{2,\ell} \in (-\pi, \pi); \phi_\ell, \theta_\ell \in \left(-\frac{\pi}{2}, \frac{\pi}{2}\right) \forall \ell. \quad (8)$$

The objective function is clearly nonconvex over ξ and is 5L-dimensional, which can be quite high if there are many multipaths. For this reason, simple local descent methods, such as gradient descent and its variations, are not effective. Additionally, the objective function computation can be quite expensive if the number of receive antennas, subcarriers, and OFDM symbols is large. The computational cost for objective function evaluation makes many global optimization methods, such as particle swarm and simulated annealing, extremely time consuming until an acceptable solution is achieved. One technique that is successful for this problem is an augmented form of alternating exact coordinate descent (AECD), further details are provided in Section V.

To perform exact coordinate descent we require that the gradient along that coordinate direction be equal to zero, e.g. for the angle of arrival of path ℓ' we have $\frac{\partial f}{\partial \phi_{\ell'}} = 0$, where f denotes the objective function in (7). Breaking down the objective function into the sum of the log-likelihood and the log-prior terms, respectively, we have $f(\xi, \mathbf{y}) = \log p(\mathbf{y}|\xi) + \log p(\xi)$. We will show that the partial derivatives of the log-likelihood term with relation to $\phi_{\ell'}$, $\theta_{\ell'}$, $\omega_{1,\ell'}$, and $\omega_{2,\ell'}$, are given by Fourier series. The series has as many terms as the size of that parameters associated dimension, e.g. $\frac{\partial \log p(\mathbf{y}|\xi)}{\partial \phi_{\ell'}}$ has N_r terms, $\frac{\partial \log p(\mathbf{y}|\xi)}{\partial \omega_{1,\ell'}}$ has N_c terms, and so on. The roots of the resulting series (including the additional prior term) will be candidate solutions for the coordinate descent update. The Fourier series root-finding problem can be turned into a companion matrix eigenvalue problem [6], we can thus readily find all roots by applying a transformation to the computed eigenvalues. Finally, we evaluate the objective on all the roots and select the one with smallest value.

We now present the partial derivatives of $\log p(\mathbf{y}|\xi)$ over the $\phi_{\ell'}$, $\theta_{\ell'}$, $\omega_{1,\ell'}$, and $\omega_{2,\ell'}$ coordinates. We omit the derivation

for space constraints. Over the following section, some indices will be arbitrarily moved from subscript to superscript in order to save space. Additionally we denote the transmitted signal at transmit antenna v as $x_{n,t}^v$.

A. Partial Derivative over $\omega_{1,\ell'}$ and $\omega_{2,\ell'}$

The partial derivative over $\omega_{1,\ell'}$ is given by

$$\frac{\partial \log p(\mathbf{y}|\boldsymbol{\xi})}{\partial \omega_{1,\ell'}} = \sum_{n=0}^{N_c-1} a_n \cos(\omega_{1,\ell'} n) + b_n \sin(\omega_{1,\ell'} n) \quad (9)$$

$$a_n = \frac{2n}{N_0} \sum_{t,u} \Im \left\{ \alpha_{\ell',n,t}^u \left(y_{n,t}^{u,*} - \sum_{\ell \neq \ell'} e^{-j\omega_{1,\ell} n} \alpha_{\ell,n,t}^{u,*} \right) \right\} \quad (10)$$

$$b_n = \frac{2n}{N_0} \sum_{t,u} \Re \left\{ \alpha_{\ell',n,t}^u \left(y_{n,t}^{u,*} - \sum_{\ell \neq \ell'} e^{-j\omega_{1,\ell} n} \alpha_{\ell,n,t}^{u,*} \right) \right\} \quad (11)$$

$$\alpha_{\ell,n,t}^u = b_\ell e^{j\omega_{2,\ell} t} e^{-j\pi u \sin(\phi_\ell)} \mathbf{a}^T(\theta_\ell) \mathbf{x}_{n,t}. \quad (12)$$

The partial derivative over $\omega_{2,\ell'}$ is similar, by symmetry.

B. Partial Derivative over $\sin(\phi_{\ell'})$

For $\phi_{\ell'}$, we take the derivative over $\sin(\phi_{\ell'})$ and exploit the bijectivity of the sine function over the $(-\frac{\pi}{2}, \frac{\pi}{2})$ range to compute the value of $\phi_{\ell'}$ that satisfies $\frac{\partial \log p(\mathbf{y}|\boldsymbol{\xi})}{\partial \sin(\phi_{\ell'})} = 0$ with smallest objective value. The partial derivative is given by

$$\frac{\partial \log p(\mathbf{y}|\boldsymbol{\xi})}{\partial \sin(\phi_{\ell'})} = \sum_{u=0}^{N_R-1} a_u \cos(\pi u \sin(\phi_{\ell'})) + b_u \sin(\pi u \sin(\phi_{\ell'})) \quad (13)$$

$$a_u = \frac{2u}{N_0} \sum_{t,n} \Im \left\{ \alpha_{\ell',n,t}^{u,*} \left(y_{n,t}^u - \sum_{\ell \neq \ell'} e^{-j\pi u \sin(\phi_\ell)} \alpha_{\ell,n,t} \right) \right\} \quad (14)$$

$$b_u = \frac{2u}{N_0} \sum_{t,n} \Re \left\{ \alpha_{\ell',n,t}^{u,*} \left(y_{n,t}^u - \sum_{\ell \neq \ell'} e^{-j\pi u \sin(\phi_\ell)} \alpha_{\ell,n,t} \right) \right\} \quad (15)$$

$$\alpha_{\ell,n,t} = b_\ell e^{j\omega_{1,\ell} n} e^{j\omega_{2,\ell} t} \mathbf{a}^T(\theta_\ell) \mathbf{x}_{n,t}. \quad (16)$$

C. Partial Derivative over $\sin(\theta_{\ell'})$

Once again, exploiting the injectivity of the sine function, we get

$$\frac{\partial \log p(\mathbf{y}|\boldsymbol{\xi})}{\partial \sin(\theta_{\ell'})} = \sum_{v=0}^{N_T-1} a_v \cos(\pi v \sin(\theta_{\ell'})) + b_v \sin(\pi v \sin(\theta_{\ell'})), \quad (17)$$

where the coefficients are given by $a_v = \frac{2}{N_0} \sum_{n,t,u} v \alpha_{n,t,u,v}$ and $b_v = -\frac{2}{N_0} \sum_{n,t,u} v \beta_{n,t,u,v}$, which in turn are expressed in terms of $\alpha_{n,t,u,v}$, given by

$$\alpha_{n,t,u,v} = \Re \left\{ \gamma_{\ell',n,t}^u \right\} \Im \left\{ x_{n,t}^v \right\} + \Im \left\{ \gamma_{\ell',n,t}^u \right\} \Re \left\{ x_{n,t}^v \right\} + |\alpha_{\ell',n,t}^u|^2 \Im \left\{ \sum_{k=v}^{N_T-1} x_{n,t}^k x_{n,t}^{k-v,*} \right\} - \Im \left\{ y_{n,t}^{u,*} \alpha_{\ell',n,t}^u x_{n,t}^v \right\}; \quad (18)$$

and $\beta_{n,t,u,v}$. For $v = 0$:

$$\beta_{n,t,u,0} = \Re \left\{ \gamma_{\ell',n,t}^u \right\} \Re \left\{ x_{n,t}^v \right\} - \Im \left\{ \gamma_{\ell',n,t}^u \right\} \Im \left\{ x_{n,t}^v \right\} + \frac{|\alpha_{\ell',n,t}^u|^2}{2} \sum_{k=0}^{N_T-1} |x_{n,t}^k|^2 - \Re \left\{ y_{n,t}^{u,*} \alpha_{\ell',n,t}^u x_{n,t}^v \right\} \quad (19)$$

and, for $v = 1, \dots, N_t - 1$:

$$\beta_{n,t,u,v} = \Re \left\{ \gamma_{\ell',n,t}^u \right\} \Re \left\{ x_{n,t}^v \right\} - \Im \left\{ \gamma_{\ell',n,t}^u \right\} \Im \left\{ x_{n,t}^v \right\} + |\alpha_{\ell',n,t}^u|^2 \Re \left\{ \sum_{k=v}^{N_T-1} x_{n,t}^k x_{n,t}^{k-v,*} \right\} - \Im \left\{ y_{n,t}^{u,*} \alpha_{\ell',n,t}^u x_{n,t}^v \right\}. \quad (20)$$

D. Optimization over $b_{\ell'}$

We assume a complex normal prior for $b_{\ell'}$, with mean $\bar{b}_{\ell'}$ and variance $\nu_{b_{\ell'}}$. It can be seen that f is convex over $b_{\ell'}$. Using Wirtinger calculus, we can derive closed form expressions for the exact coordinate update on $b_{\ell'}$, for a single ℓ' (even though a closed form joint update for $b_{\ell'} \forall \ell'$ exists by solving a linear system). We once again omit the derivation, presenting only the result

$$b_{\ell'}^{\text{opt}} = \frac{\nu_{b_{\ell'}} \sum_{n,t,u} \gamma_{\ell',n,t}^{u,*} \left(y_{n,t}^u - \sum_{\ell \neq \ell'} b_{\ell'} \gamma_{\ell,n,t}^u \right) + N_0 \bar{b}_{\ell'}}{\nu_{b_{\ell'}} \sum_{n,t,u} |\gamma_{\ell',n,t}^u|^2 + N_0}, \quad (21)$$

where $\gamma_{\ell,n,t,u} = e^{j\omega_{1,\ell} n} e^{j\omega_{2,\ell} t} e^{-j\pi u \sin(\phi_\ell)} \mathbf{a}^T(\theta_\ell) \mathbf{x}_{n,t}$.

E. Priors

Because we want to preserve the Fourier series structure of the partial derivatives, we must choose priors which have derivatives that can be directly incorporated into a Fourier series. For $\omega_{1,\ell}$, we consider the following prior distribution

$$p(\omega_{1,\ell}) \propto \exp \left(-\frac{|e^{j\bar{\omega}_{1,\ell} n} - e^{j\omega_{1,\ell} n}|^2}{\nu_{\omega_{1,\ell}}} \right), \quad (22)$$

where $\bar{\omega}_{1,\ell} \in (-\pi, \pi)$ and $\nu_{\omega_{1,\ell}} > 0$ respectively denote the mode and variance parameter. Note that, while the mode of the distribution is indeed equal to $\bar{\omega}_{1,\ell}$, the variance is merely an increasing function of $\nu_{\omega_{1,\ell}}$. A similar prior is used for $\omega_{2,\ell}$. For ϕ_ℓ we use

$$p(\phi_\ell) \propto \exp \left(-\frac{|e^{j\pi \sin(\bar{\phi}_\ell)} - e^{j\pi \sin(\phi_\ell)}|^2}{\nu_{\phi_\ell}} \right), \quad (23)$$

with mode and variance parameters similarly defined. The proposed prior for θ_ℓ is identical. The path gain coefficient prior has been already introduced in Subsection IV-D. In sequential estimation, the mode of the current estimation step corresponds to the point estimates of the previous step, the variance however must be heuristically chosen.

F. Partial Derivative of the Priors

The presented partial derivatives include only the log-likelihood term. We must add the log-prior to have the complete objective. The derivative of the log-prior of $\phi_{\ell'}$ is

$$\frac{\partial \log p(\boldsymbol{\xi})}{\partial \sin(\phi_{\ell'})} = -\frac{2\pi}{\nu_{\phi_{\ell'}}} \sin(\pi \sin(\bar{\phi}_{\ell'})) \cos(\pi \sin(\phi_{\ell'})) + \frac{2\pi}{\nu_{\phi_{\ell'}}} \cos(\pi \sin(\bar{\phi}_{\ell'})) \sin(\pi \sin(\phi_{\ell'})). \quad (24)$$

A similar equation applies for $\theta_{\ell'}$, by symmetry. For $\omega_{1,\ell'}$ we have

$$\frac{\partial \log p(\boldsymbol{\xi})}{\partial \omega_{1,\ell'}} = \frac{2 \cos(\bar{\omega}_{1,\ell'}) \sin(\omega_{1,\ell'})}{\nu_{\omega_{1,\ell'}}} - \frac{2 \sin(\bar{\omega}_{1,\ell'}) \cos(\omega_{1,\ell'})}{\nu_{\omega_{1,\ell'}}}. \quad (25)$$

Again, the expression for $\omega_{2,\ell'}$ follows by symmetry. By adding these terms to the partial derivatives of the log-likelihood term we get the partial derivative of the objective.

V. OPTIMIZATION PROCEDURE

For the inference problem above, the gradient or coordinate descent methods by themselves are ineffective in providing acceptable solutions. Also, due to the dimensions and evident nonconvexity of the optimization problem, proving optimality of the solutions is hard. To achieve a useful feasible solution, we propose an AECD method, in which the parameters for a single multipath index are optimized in an exact alternating fashion in an inner loop, while the outer loop varies the current multipath index. Because the exact coordinate descent is still a local descent method, we augment it with a combination of momentum and a successive over-relaxation (SOR) inspired coordinate update, this is essential to escape local optima and improve the estimation results.

Let us first detail the outer and inner loop structure. First, a maximum number of expected paths L_{\max} is defined. This number should be surely larger than the possible number of detectable paths, i.e., paths with power that is not much smaller than the noise variance, and depends heavily on the propagation characteristics of the environment. The outer loop progresses along path indices in the following order:

$$\mathbf{I} = [1, 2, 1, 2, 3, 1, 2, 3, 4, \dots, L_{\max} - 1, L_{\max}, 1, \dots, L_{\max}]. \quad (26)$$

Intuitively, after the first path is detected and roughly estimated, the algorithm moves on to detect the next path. Once the next path is detected and estimated, then the algorithm returns to the first path such as to ‘‘compensate the interference’’ of the previously undetected second path when estimating the first path. This reasoning proceeds until hopefully all paths up to L_{\max} have been estimated. If at some point of the outer loop no more paths remain, then the algorithm starts outputting spurious paths, which have no physical correspondence. This means that choosing a large value for L_{\max} has a time cost, as the algorithm would have to estimate many spurious paths before finishing. It is convenient to devise a procedure to detect when all true paths have already been detected.

Moving on to the inner loop. Suppose that the current path at the outer loop is ℓ' , then, in a single iteration, the coordinates are updated in the following order: $b_{\ell'}$, $\omega_{1,\ell'}$, $b_{\ell'}$, $\omega_{2,\ell'}$, $b_{\ell'}$, $\theta_{\ell'}$, $b_{\ell'}$, $\phi_{\ell'}$. The inner loop is repeated for a maximum set amount of iterations it_{\max} . Updating the path coefficient $b_{\ell'}$ in-between the other coordinates apparently provides more efficient updates. Exploring this idea, for future work, it may be effective to define a ‘‘new’’ objective function by direct substitution of the optimal paths using (21) on (5), and then attempt to optimize this function.

Finally, we describe the individual coordinate updates. Denote by ξ_m the coordinate to be updated for the m th time, also denote by ξ_m^{opt} its optimal coordinate descent update. Then its partial update with momentum is

$$\xi'_{m+1} = \xi_m^{\text{opt}} + \eta_m(\xi_m - \xi_{m-1}), \quad (27)$$

where η_m is the momentum coefficient of that variable at the m th update. We then perform a SOR inspired rule to complete the coordinate update

$$\xi_{m+1} = \text{Wrap}_{\xi}((1 - \lambda_m)\xi_m + \lambda_m \xi'_{m+1}), \quad (28)$$

where $\lambda_m \in [0.5, 1.5]$ is the SOR coefficient of that variable at update m , and $\text{Wrap}_{\xi}(\cdot)$ denotes wrapping the argument value to the valid domain of the parameter, e.g., ϕ and θ should be wrapped to the interval $(-\frac{\pi}{2}, \frac{\pi}{2})$ and ω_1 and ω_2 to $(-\pi, \pi)$. Because each variable is updated with forward substitution (like a Gauss-Seidel update for solving linear equations), instead of updating all coordinates together (like a Jacobi update), we apply a heuristic form of SOR, which is known to outperform the Gauss-Seidel for linear equations. While there are no theoretical convergence speed guarantees, it provides an additional degree of freedom to tune the algorithm.

Algorithm 1 Multipath parameter estimation algorithm.

```

1: procedure ESTIMATEPARAMS( $\mathbf{y}$ ,  $L_{\max}$ ,  $\hat{\boldsymbol{\xi}}_{i-1}$ )
2:    $l = 1$ ;
3:   for  $\ell = \mathbf{I}[l]$  do    ▷ Path order  $\mathbf{I}[l]$  as in defined (26)
4:     Initialize  $\boldsymbol{\xi}_{\ell} = \mathbf{0}$ ;
5:     for  $it = 1, \dots, it_{\max}$  do
6:       Compute objective  $f_0 = f(\boldsymbol{\xi}, \mathbf{y})$ ;
7:       Update coordinates in the order:  $b_{\ell}$ ,  $\omega_{1,\ell}$ ,  $b_{\ell}$ ,
        $\omega_{2,\ell}$ ,  $b_{\ell}$ ,  $\theta_{\ell}$ ,  $b_{\ell}$ , using (27) and (28);
8:       Compute objective  $f_1 = f(\boldsymbol{\xi}, \mathbf{y})$ ;
9:       if  $|\Delta(\boldsymbol{\xi}_{\ell})| < \epsilon_{\text{var}}$  then
10:        Break;
11:      else if  $f_1 - f_0 < \epsilon_{\text{obj}}$  then
12:        Break;
13:      else if Other stopping heuristics then
14:        Break;
15:       $l = l + 1$ ;
16:    Estimate  $\hat{L}$ ;
17:  return  $\boldsymbol{\xi}$ ;
```

Algorithm 2 Algorithm for the estimation of the number of active paths.

```

1: procedure ESTIMATE_L( $\mathbf{y}$ ,  $\hat{\boldsymbol{\xi}}_i$ ,  $\epsilon_L$ )
2:   Sort  $\hat{\boldsymbol{\xi}}_{\ell}$  in decreasing  $|b_{\ell}|$  order, for  $\ell = 1, \dots, L_{\max}$ ;
3:   Save sorting order in vector  $\mathbf{S} = [s_1, \dots, s_{L_{\max}}]$ 
4:   for  $i = 1, \dots, L_{\max}$  do
5:     Compute objective  $f_i = f(\boldsymbol{\xi}_{s_1}, \dots, \boldsymbol{\xi}_{s_i}, \mathbf{y})$ 
6:   for  $i = 1, \dots, L_{\max}$  do
7:     if  $f_i - f_{i+1} < \epsilon_L \frac{(f_1 - f_i)}{i}$  then
8:       return  $i$ ;
9:   return  $L_{\max}$ ;
```

An outer loop iteration may be interrupted and skipped if the estimates have failed to change by the desired amount in an inner loop iteration, e.g., if all parameters have not changed by more than 10^{-5} . An outer loop iteration may also be skipped if the objective function has not changed by more than a threshold for a particular inner iteration. Given a set of multipath parameters from a previous estimation $\hat{\xi}_{i-1}$, a basic outline of the proposed algorithm is provided in Algorithm 1. In Algorithm 1, ξ_ℓ denotes the variables associated with path ℓ , $\Delta(\xi_\ell)$ denotes the vector of relative changes of all variables from path ℓ , the inequality $|\Delta(\xi_\ell)| \prec \epsilon_{\text{var}}$ denotes that all relative changes are less than the threshold ϵ_{var} . Similarly, ϵ_{obj} is the threshold for objective change in a single iteration. One may consider using additional stopping heuristics such as keeping track of a trailing moving average, if some property of the moving average indicates slow convergence, then break and move on to the next outer loop iteration.

Line 16 of Algorithm 1 requires estimating the number of paths. For this, we propose a method based on objective function decrease. It consists first sorting paths in decreasing order based on the estimated path powers $|b_\ell|$, then progress through the vector by including more paths, computing the objective function, and checking how much the objective decreased by including the last path. Proceed until a (possibly variable) threshold value is reached. The version used in Section VI is displayed in Algorithm 2.

VI. NUMERICAL RESULTS

In this section, we will assess the performance of the proposed method by analysing simulation results. Initially, we want to verify how effectively the algorithm detects the existing paths without any prior information. Then, we present a simple example of how this algorithm can be used for mapping, given perfectly known positions and orientations (poses) of the transmitter (UE) and receiver (BS). In both scenarios, we consider a transmitted pilot signal with 50 OFDM symbols and 40 subcarriers. The transmitter and receiver have ULAs with 4 and 16 antennas, respectively. The used carrier frequency is 60 GHz, the subcarrier spacing is 240 kHz, and the symbol time is $4.46 \mu\text{s}$, which corresponds to numerology $\mu = 4$ in the 5G standard. The channel simulation considers only first order specular reflections. Paths with angles of arrival or departure outside the $(-\frac{\pi}{2}, \frac{\pi}{2})$ interval are considered to have zero gain. The environment used in this section is depicted in Fig. 1. For space constraints, we leave a detailed comparison with other methods [2]–[4] for future work.

We introduce a channel model with the intention of offering a sufficient geometrical representation of multipath propagation for our estimation problems. The path coefficient is computed from the total propagation distance d_ℓ^2 with an added power reflection loss $0 < c_\ell < 1$ if the path is not line-of-sight (LOS), given by $|b_\ell| = \sqrt{c_\ell/(4\pi d_\ell^2)}$. We consider the transmit power P_T to be equally allocated to all subcarriers N_c . Naturally, if the path is LOS, then $c_\ell = 1$. The reflection coefficient for non-line-of-sight (NLOS) paths is set to $c_\ell = 0.2$. The phase is sampled from a uniform distribution

$\angle b_\ell \sim \mathcal{U}(-\pi, \pi)$, thus $b_\ell = |b_\ell|e^{j\angle b_\ell}$. The ToFs are simply the path distance divided by the speed of light $\tau_\ell = d_\ell/c$. The Doppler frequency is computed from the projection of the UE velocity on the departure direction vector v_ℓ , and is given by $f_{D,\ell} = f_{\text{carrier}}v_\ell/c$. We consider a $\tau_o = 0.1 \mu\text{s}$ clock offset between UE and BS. The carrier frequency offset is set to 2.4 MHz, 40 ppm of the carrier frequency.

For the model to be identifiable, the transmitted signal cannot be arbitrarily chosen. Intuitively, AoD estimation requires that different angles of departure produce distinguishable outputs throughout the pilot sequence. It is impossible to estimate θ_ℓ if a single data stream is transmitted with a fixed precoder. Using more data streams is one way to ensure that it is possible to estimate the AoD. In the uplink context, it is not usual to transmit many streams. By transmitting a single stream, but varying the precoder, it is possible to guarantee identifiability. We consider 1 data stream and a time-varying precoder matched to angle $\bar{\theta} \in (-\frac{\pi}{2}, \frac{\pi}{2})$, which is uniformly swept from $-\frac{\pi}{2}$ to $\frac{\pi}{2}$ during the 50 OFDM symbols.

Given no prior, we want to assess the precision and recall of the path detection and estimation. We simulate 1024 different scenarios, with random UE poses and BS at (5, 30). The transmitter positions are uniformly distributed on the $[1, 19] \times [1, 19]$ rectangle, while their orientation is uniformly distributed on the $\psi_{\text{UE} \rightarrow \text{BS}} + [-\pi/2, \pi/2]$ interval, where $\psi_{\text{UE} \rightarrow \text{BS}}$ is the orientation where the UE perfectly faces the BS. Transmit power is set to 8 W, i.e., 9 dBW, equally divided along all subcarriers so that each subcarrier has -7 dBW. Noise power is set to -80 dBW. For the optimizer parameters, we set $L_{\text{max}} = 6$, and the thresholds to $\epsilon_{\text{var}} = 10^{-5}$ and $\epsilon_{\text{obj}} = 10^{-6}$. The momentum coefficients are initialized to 0.1 and are decremented at every inner loop iteration with the rule $\eta_{m+1} = 0.99\eta_m$. The SOR coefficients are updated at every inner loop iteration with the

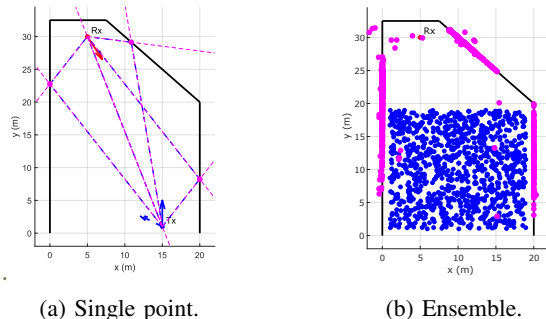


Fig. 1: Geometric channel simulation environment. The walls are represented by black lines, the propagation paths are indicated by blue dashed lines, the magenta dashed lines are the propagation directions of the signal computed from the angle of arrival (AoA) and angle of departure (AoD) estimates (given perfect UE and BS pose information). The red/blue dot and arrow indicate the position and orientation of the BS/UE, respectively. The magenta dots are the intersection of the magenta lines, this is one way of estimating the reflector positions. The dashed blue line shows the transmitter velocity.

following rule $\lambda_{it} = 0.98 + 0.22 \exp\left(-\frac{it}{15}\right)$, where “it” is the inner loop iteration counter. The threshold for Algorithm 2 is $\epsilon_L = 0.5$. An example of the estimation results in this setup is represented by the magenta lines in Fig. 1a. The full ensemble of points is shown in Fig. 1b.

It may happen that some paths do not converge but are still declared to be valid paths by our algorithm. To determine how frequently this happens, we compare the estimated paths to the true paths by computing $\|\xi_\ell - \hat{\xi}_\ell\|_2$ and performing greedy assignment. The estimated paths that had no assigned true paths were considered misdetections. On the other hand, estimated paths that were properly assigned to a true path were considered true detections. This way it is possible to estimate the Precision and Recall of our algorithm. Following the described procedure yields precision of 0.9938 and recall of 0.9854. The estimates of true detections have their mean squared error (MSE) and root mean squared error (RMSE) values shown in Table I. It can be seen that, ignoring misdetections, the quality of estimates is quite useful, particularly for the ω_1 and ω_2 values as well as the path magnitude $|b_\ell|$. The estimates for the angles of departure and arrival are not as good, but are still sufficient for approximately sensing the environment, given perfect transmitter pose information. Using ω_1 and ω_2 requires very fine clock and carrier synchronization to eliminate the offsets and extract useful geometric information.

TABLE I: MSE and RMSE for the parameter estimates of valid paths, maximum likelihood (ML) estimation

	$ b_\ell $	$\angle b_\ell$	ϕ_ℓ	θ_ℓ	$\omega_{1,\ell}$	$\omega_{2,\ell}$
MSE	5.5E-7	0.0241	0.0146	0.0191	4.5E-6	1.9E-4
RMSE	7.4E-4	0.1554	0.1210	0.1383	0.0021	0.0139

Finally, we explore the sequential estimation scenario, in which the estimates from the previous instant are used as priors for the next estimation round. The path of the transmitter and the estimated position of reflectors using the line intersection method is shown in Fig. 2. The whole path is traveled over 5 seconds with 50 estimation rounds performed in equal time intervals. We set all variance parameters to $\nu = 0.005$ and achieve 1 precision 0.9844 recall. The equivalent ML precision and recall are 0.9844 and 0.9844, respectively. The MSE and the RMSE values for MAP and ML in this scenario are presented in Table II. Besides the improved precision and recall and similar MSE values, the MAP also converges faster, which can be beneficial in real time applications. It is up to the user to decide the best approach for the intended use.

TABLE II: MSE and RMSE for the parameter estimates of valid paths, MAP and ML estimation.

	$ b_\ell $	$\angle b_\ell$	ϕ_ℓ	θ_ℓ	$\omega_{1,\ell}$	$\omega_{2,\ell}$
MSE (MAP)	1.2E-6	0.1023	0.0093	0.0048	1.8E-5	1.0E-3
RMSE (MAP)	0.0011	0.3198	0.0964	0.0691	0.0043	0.0319
MSE (ML)	1.2E-6	0.0837	0.0093	0.0050	1.8E-5	6.2E-4
RMSE (ML)	0.0011	0.2894	0.0964	0.0708	0.0043	0.0250

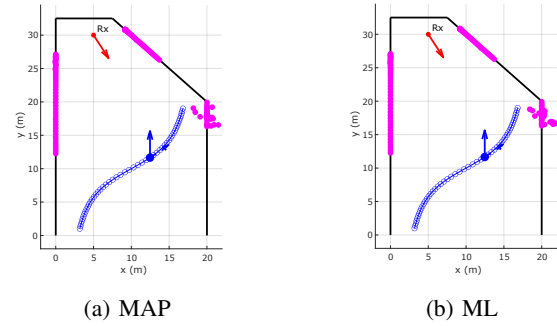


Fig. 2: Environment and transmitter trajectory, UE orientation is always facing north, i.e., 90° , BS orientation is the same as in the first simulation. An example sample point is shown.

VII. CONCLUSION

Estimating all the multipath components and their parameters is not a simple problem, and existing methods frequently rely on many simplifications or extensive computation that hinders its real-time applicability. In this paper, we have introduced a ML and MAP estimation procedure for channel estimation with possible use cases in sensing and mapping using an OFDM waveform. The proposed method specifically exploits the problem structure and can be improved in straightforward fashion to provide increased robustness, efficiency, accuracy and detection capabilities.

ACKNOWLEDGEMENTS

The work was supported in part by the Research Council of Finland (former Academy of Finland) 6G Flagship Program (Grant Number: 346208) and 6GWiCE project (357719). We would also like to thank Hamza Djelouat, Mikko Sillanpää, and Reijo Leinonen for the productive discussions.

REFERENCES

- [1] D. K. Pin Tan, J. He, Y. Li, A. Bayesteh, Y. Chen, P. Zhu, and W. Tong, “Integrated Sensing and Communication in 6G: Motivations, Use Cases, Requirements, Challenges and Future Directions,” in *2021 1st IEEE Int. Online Symp. on Joint Commun. & Sensing (JC&S)*, 2021, pp. 1–6.
- [2] B. Fleury, M. Tschudin, R. Heddergott, D. Dahlhaus, and K. Ingeman Pedersen, “Channel parameter estimation in mobile radio environments using the SAGE algorithm,” *IEEE Journal on Selected Areas in Communications*, vol. 17, no. 3, pp. 434–450, 1999.
- [3] F. Wen, J. Kulmer, K. Witrisal, and H. Wymeersch, “5G Positioning and Mapping With Diffuse Multipath,” *IEEE Trans. Wireless Commun.*, vol. 20, no. 2, pp. 1164–1174, 2021.
- [4] Z. Zhou, J. Fang, L. Yang, H. Li, Z. Chen, and S. Li, “Channel Estimation for Millimeter-Wave Multiuser MIMO Systems via PARAFAC Decomposition,” *IEEE Trans. Wireless Commun.*, vol. 15, no. 11, pp. 7501–7516, 2016.
- [5] J. A. Zhang, M. L. Rahman, K. Wu, X. Huang, Y. J. Guo, S. Chen, and J. Yuan, “Enabling Joint Communication and Radar Sensing in Mobile Networks—A Survey,” *IEEE Commun. Surveys Tuts.*, vol. 24, no. 1, pp. 306–345, 2022.
- [6] J. Boyd, “Computing the zeros, maxima and inflection points of Chebyshev, Legendre and Fourier series: Solving transcendental equations by spectral interpolation and polynomial rootfinding,” *J. of Eng. Math.*, vol. 56, pp. 203–219, 11 2006.